

# Metallic helix array as a broadband wave plate

Chao Wu, Hongqiang Li,\* Xing Yu, Fang Li, and Hong Chen

*Key Laboratory of Advanced Micro-structure Materials, MOE,  
Department of Physics, Tongji University, Shanghai 200092, China*

C.T. Chan

*Department of Physics, Hong Kong University of Science and Technology,  
Clear Water Bay, Kowloon, Hong Kong, China*

## Abstract

This study proposes that a metallic helix array can operate as a highly-transparent broadband wave plate in propagation directions perpendicular to the axis of helices. The functionality arises from a special property of the helix array, namely that the eigenstates of elliptically right-handed and left-handed polarization are dominated by Bragg scattering and local resonance respectively, and can be modulated separately with nearly fixed difference between their wavevectors in a wide frequency range. The wave plate functionality is theoretically and experimentally demonstrated by the transformation of polarized states in a wide frequency range.

---

\* hqlee@tongji.edu.cn

Manipulating the polarization of electromagnetic (EM) wave is instrumental in both fundamental optical physics and photonics applications. A wave plate, in the form a birefringent crystal with specific orientation and thickness, has long been used for the purpose of polarization control. It transforms the polarization of electromagnetic waves by the superposition of two linearly polarized states that are orthogonal to each other propagating inside the crystal with different phase velocity [1]. The two orthogonal states can also be, alternatively, left-handed and right-handed elliptically polarized (LEP and REP) eigenstates of uniaxial bianisotropic medium [2]. It is worth noting that, such a wave plate with a certain thickness can only operate in a narrow frequency range [1, 2] as the difference of phase velocity of two polarized eigenstates is frequency dependent. A broadband wave plate requires that, not only the difference of phase velocity but also the axis ratios of the two polarized states must not change throughout the whole operational band. To the best of our knowledge, no natural or artificial medium exhibits such properties.

Metamaterials have great potential in offering a variety of novel functionalities, such as negative refraction [3], super lens [4, 5] invisibility cloak [6, 7], and polarization control via chiral route [8–12]. The concept of metamaterial presents a paradigm to create novel electromagnetic materials in a form of artificial meta-atom ensemble [13, 14]. Crux of the matter relies on how to tailor the electromagnetic responses and mutual coupling between the electric field and magnetic field in metamaterial [15]. However, the most of metamaterials only operate in a narrow frequency range due to local resonance nature. One goal to be achieved is to find metamaterial alternatives for related photonic devices with superior performance much beyond the natural material limits. A helix array, as one classical representative in chiral metamaterials, is also very unique in that the electromagnetic properties of such kind of structure are the collective effect between the local resonance that governs metamaterials and Bragg scattering that governs photonic crystals [16–18].

In this paper, we show that the helical symmetry of helices provides additional degrees of freedom for tuning the dispersion branches in different handedness, namely the REP and LEP eigenstates on the transverse plane of metallic helix array are dominated separately by Bragg scattering and local resonance arising from the continuous helical symmetry. The ellipticity and difference between wavevectors of the two states can be fixed in a wide frequency range by choosing appropriate geometric parameters, leading to a helix solution for highly transparent broadband wave plate. The proof-of-principle experiments in microwave

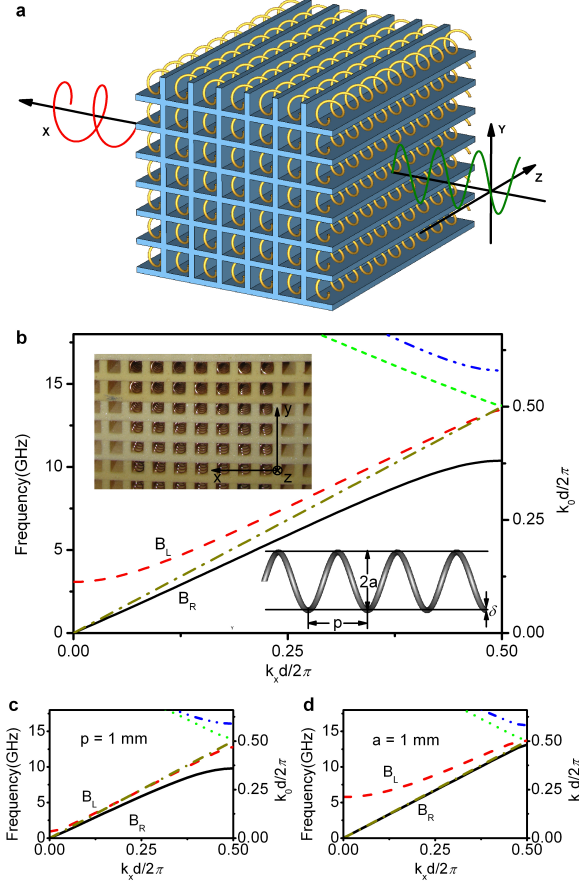


FIG. 1. A Slab of Helices as Wave Plate for Transversely Propagating Waves. (a) The schematic configuration of transverse propagation through helices, the helices are arranged in a square array; (b) the photo of the 7-layered sample and the corresponding dispersion diagram  $\omega(k_x, k_y = k_z = 0)$ . The geometric parameters are the pitch  $p = 4$  mm, helix radius  $a = 3$  mm, wire diameter  $\delta = 0.6$  mm, the lattice constant  $d = 11$  mm; and the comparative results by (c) varying pitch only to  $p = 1$  mm, and (d) varying helix radius only to  $a = 1$  mm, all other parameters are fixed to their respective values in Fig. 1(b).

regime verify the theoretical calculations very well. The thickness-dependent character of wave plate is also verified by the calculated and measured transmission spectra of other model samples with different thickness. This is a first realization of a broadband wave plate which utilizes the LEP and REP states of metallic helix array.

Figure 1 presents the schematic configuration on how a slab of right-handed (RH) metallic helix array operates as a wave plate [Fig. 1(a)], the photo of the 7-layered slab sample, the corresponding dispersion diagram  $\omega(k_x, k_y = k_z = 0)$  [Fig. 1(b)], and the comparative results

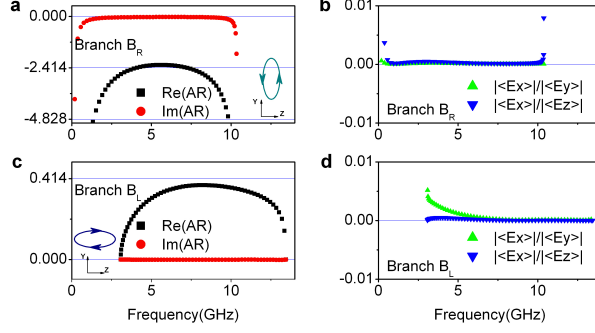


FIG. 2. Polarization Characters of Eigenmode. Axial ratio  $AR = \langle E_y \rangle / \langle iE_z \rangle$ , and longitudinal ratios  $|\langle E_x \rangle| / |\langle E_y \rangle|$ ,  $|\langle E_x \rangle| / |\langle E_z \rangle|$  are calculated for (a), (b)  $B_R$ , and (c), (d)  $B_L$  modes. Black squares for  $Re(AR)$ , red circles for  $Im(AR)$ , green up-triangles for  $|\langle E_x \rangle| / |\langle E_y \rangle|$ , and blue down-triangles for  $|\langle E_x \rangle| / |\langle E_z \rangle|$ .  $\langle \dots \rangle$  denotes the spatial average in a unit cell.

by varying critical parameters associated with helical symmetry and Bragg scattering [Fig. 1(c) and (d)]. The geometric parameters of the sample shown in Fig. 1(b) are the pitch  $p = 4$  mm, the helix radius  $a = 3$  mm, the wire diameter  $\delta = 0.6$  mm, and the lattice constant  $d = 11$  mm. As the helical symmetry requires that a RH helix comes back to itself after being translated by a distance of  $\Delta z$  and being rotated simultaneously by an angle of  $2\pi\Delta z/p$  with  $p$  being the pitch size, the field components for an RH helix system can be expanded by functions of the form, i.e. the helical Bloch states, as  $\psi_n(\rho, \varphi, z) = e^{ik_z z} F_n(\rho) e^{-in\varphi + 2n\pi z/p}$ , where  $k_z$  is the Bloch wave vector along  $z$  axis, and  $n$  is the Bloch order associated with angular momentum [18]. Our calculations show that the lowest branch  $B_R$  [black solid line in Fig. 1(b)] is dictated by the degenerate  $\pm 1^{st}$  orders of helical Bloch states, while the second lowest branch  $B_L$  [red dashed line in Fig. 1(b)] is dictated by the  $0^{th}$  order of helical Bloch state. The polarization characters of eigenstates are calculated and illustrated in Fig. 2, shown as the longitudinal ratios  $|\langle E_x \rangle| / |\langle E_y \rangle|$ ,  $|\langle E_x \rangle| / |\langle E_z \rangle|$  and the axis ratio  $AR = \langle E_y \rangle / \langle iE_z \rangle$  of the  $B_L$  and  $B_R$  states, where  $\langle \dots \rangle$  refers to the spatial average inside a unit cell. We see from Fig. 2 that,  $B_R$  states pick up an REP character with long axis along the  $z$  axis, while the  $B_L$  states pick up an LEP character with long axis along the  $y$  axis. These properties are essentially decided by the helical Bloch states, since the  $0^{th}$  order helical Bloch states have their fields primarily guided along the helix axis, while the  $\pm 1^{st}$  orders of helical Bloch states have their fields restricted on the transverse plane. The electric field of two orthogonal elliptical states  $|\varphi_{LEP}\rangle$  and  $|\varphi_{REP}\rangle$  propagating along  $x$  axis

can be expressed as

$$E_{REP} = (\alpha u_y + i\beta u_z) e^{i(k_{REP}x - \omega t)} \quad (1)$$

$$E_{LEP} = (\beta u_y - i\alpha u_z) e^{i(k_{LEP}x - \omega t)} \quad (2)$$

where  $\alpha$  and  $\beta$  are two different positive numbers that determines the axis ratio of the elliptical states,  $u_y$  and  $u_z$  denote the unitary vectors along the  $y$  and  $z$  coordinate axes.

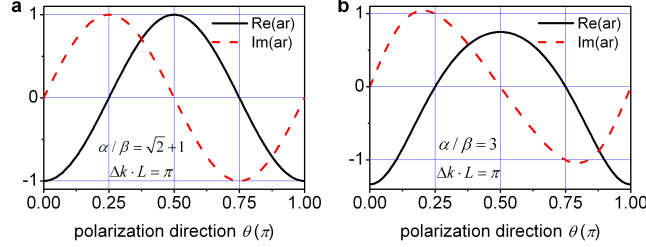


FIG. 3. Polarization Transformation. Axial ratio  $ar$  of the transmitted waves as a function of the polarization angle of linearly polarized incidence when the slab thickness satisfies to  $\Delta k \cdot L = \pi$  and the ellipticity of the eigenstates is at (a)  $\alpha/\beta = \sqrt{2} + 1$  or (b)  $\alpha/\beta = 3$ . The ratio  $ar$  is defined as  $ar = E_y/iE_z$ , similar to the axial ratio for eigenstates illustrated in Fig. 2.

A salient feature of the band structure shown in Fig. 1(b) is that the  $B_L$  and  $B_R$  branches are essentially linear and parallel to each other in a wide frequency range of 3.9 GHz  $\sim$  9.6 GHz. Within this band, two orthogonal eigenstates  $|\varphi_{LEP}\rangle$  and  $|\varphi_{REP}\rangle$  of the  $B_L$  and  $B_R$  branches pick up the same difference  $\Delta k = k_{LEP} - k_{REP}$  between their wavevectors. This property generally holds for all directions in the transverse plane, leading to a circular equi-frequency surface in a wide frequency range, as if the helix array behaves as an isotropic medium for the transversely propagating waves. We also note that the axial ratio of the in-plane field components for the LEP/REP branch is roughly fixed within the same frequency range as well (see Fig. 2). The findings are adequate for producing a broadband wave plate which surpasses the narrow bandwidth limitation.

The feature in dispersion diagram that two branches are in parallel to each other in a wide frequency range is not likely to be found in other systems. We see from Fig. 1(b) that the branch  $B_R$  is nearly linear at small values of wavevector  $k_x$  as it is primarily dominated by Bragg scattering. A Bragg gap is opened up at Brillouin zone (BZ) boundary between the  $B_R$  branch and the fourth branch (blue dash-dot line) in the same handedness. On the other hand, the branch  $B_L$ , in a locally resonant manner with a cut-off frequency at  $k_x = 0$ ,

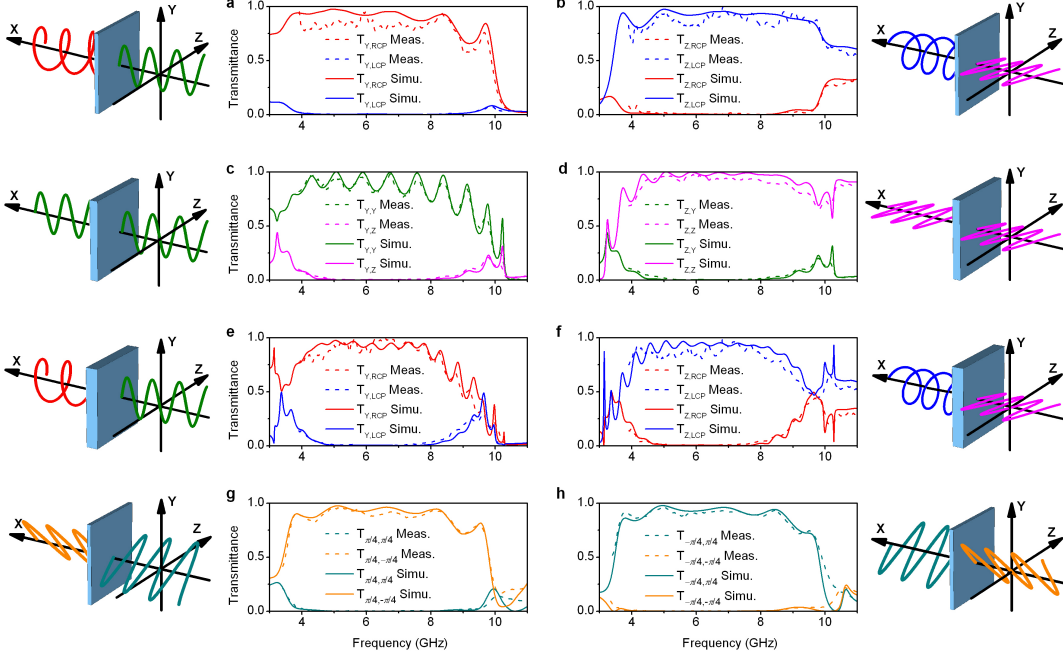


FIG. 4. Transmission Spectra of Helix Samples as Wave Plate. Transmission spectra are calculated and measured for three samples with 7, 14 and 21 periods along the propagating direction ( $x$ -direction). (a) and (b), (g) and (h) for 7-period sample, (c) and (d), (e) and (f) for 14-, 21-period samples, respectively. The first and the second subscripts,  $i$ , and  $j$ , of the transmission spectra  $T_{i,j}$  refers to the polarized state of the incident and the transmitted waves, respectively. The letter Y or Z denotes a linear polarization along  $y$ - or  $z$ - direction. The symbol  $\pi/4$  or  $-\pi/4$  denotes linear polarization with a polarization angle at  $\pi/4$  or  $-\pi/4$  about  $y$ - axis. RCP or LCP denotes a right-handed or left-handed circular polarization. The transmission spectra are normalized to the total power of the incidence.

becomes linear quickly with the increase of  $k_x$  as the  $B_L$  states are nearly free from Bragg scattering. If we only decrease the pitch, for example, to  $p = 1$  mm as shown in Fig. 1(c), the cut-off frequency of the  $B_L$  branch at  $k_x = 0$  (which is primarily determined by helical symmetry) falls down to a rather low frequency. Meanwhile the lineshape of  $B_R$  branch is almost not changed as it can hardly see the chiral feature. And now the slope of the  $B_L$  branch becomes larger than that of the  $B_R$  branch [see Fig. 1(c)]. It is also worth noting that our helix system adopting a smaller size of radius  $a$  tends to regress to an array of thin metallic wires, and the cut-off frequency of the  $B_L$  branch goes higher rapidly, while the  $B_R$  branch becomes more asymptotic to light line due to weak Bragg scattering effect as the

filling ratio of metallic helices is small. And the slope of the  $B_L$  branch will decrease and can be apparently smaller than that of the  $B_R$  branch as shown in Fig. 1(d).

The eigenstate analysis provides intuitive information for interpreting the phenomena that the  $B_L$  and  $B_R$  branches can be modulated independently. A  $B_L$  state is primarily dictated by the  $0^{th}$  order helical Bloch state with its long axis along  $z$  direction (helical axis) as shown in Fig. 2. Such a state, almost free from the in-plane Bragg scattering, reveals a resonant character arising from mutual coupling between the electric field and magnetic field along helical axis. On the other hand, as a  $B_R$  eigenstate is primarily dictated by the  $\pm 1^{st}$  orders of degenerate helical Bloch states with  $y$  direction as its long axis (see Fig. 2), the major field components are reserved along the axial direction. And the state is heavily modulated by Bragg-scattering channels in  $xy$  plane instead of mutual coupling between electric and magnetic fields along the axial direction. As a consequence, the two branches, almost independently modulated by the electromagnetic mutual coupling along helical axis and the Bragg-scattering in transverse plane, respectively, can be tuned separately [19] to be essentially in parallel to each other, given an appropriate set of geometric parameters like those illustrated in Fig. 1(b). The ellipticity of eigenstates can also be tailored much in the same way.

Consider, for example, a linearly polarized plane wave propagating along  $x$  direction through the helices with a polarization angle of  $\theta$  with respect to  $y$ -axis [see Fig. 1(a)]. The polarization of the outgoing wave [2] can be identified by its axial ratio  $ar = E_y/iE_z$  as

$$ar = \frac{(i\alpha/\beta + \tan \theta) e^{i\Delta k \cdot L} + (i\beta/\alpha - \tan \theta)}{-(i + \beta/\alpha \tan \theta) e^{i\Delta k \cdot L} + (i - \alpha/\beta \tan \theta)} \quad (3)$$

where  $L$  is the slab thickness. The transmitted waves will be transformed to be right-handed (left-handed) circularly polarized at  $\theta = 0$  ( $\theta = \pi/2$ ) provided that the axial ratios of REP and LEP eigenstates and the thickness of helix slab satisfy to  $\alpha/\beta = \sqrt{2} + 1$  and  $\Delta k \cdot L = \pi$ , as shown in Fig. 3(a). And the sample shown in the inset of Fig. 1(b), which has 7 periods along  $x$  direction, is rightly the realization of such a wave plate with appropriately designated geometric parameters. The wave plate utilizing REP and LEP states is versatile in utility. We would further address that such a helix slab can also rotate linear polarization. At the conditions  $\Delta k \cdot L = \pi$  and  $\theta = \pm\pi/4$ , the transmitted wave is still linearly polarized but with rotated polarization direction along  $\mp\pi/4$ . This property is independent from the axial ratio of elliptical eigenstates as revealed in Fig. 3 (a) and (b). In contrast, a conventional

wave plate is incapable of implementing aforementioned two different kinds of polarization transformation simultaneously.

According to the calculated band structure in Fig. 1(b), the thinnest wave plate for linear-to-circular polarization transformation (or vice versa) only requires 7 periods along the  $x$  direction. A 7-period sample slab is fabricated by periodically embedding the right-handed metallic helices in a polyurethane foam slab. The polyurethane foam slab is lossless with a dielectric constant of  $\varepsilon \approx 1.01$ . The sample slab contains  $7 \times 60$  metallic helices (i.e. 7 periods along the  $x$ -direction and 60 periods along the  $y$ -direction), each helix has 200 periods along the helical axis ( $z$ -direction). For comparison, finite-difference-in-time-domain algorithm is performed to calculate the transmission spectra. Calculations show that the transmitted waves are transformed to right-handed or left-handed circular polarization (RCP or LCP), respectively, under  $y$ -polarized or  $z$ -polarized incidence as shown with the solid lines in Figs. 4(a) and 4(b). The calculated transmittance is above 90% at the most of the frequencies in the range of  $3.9 \sim 9.6$  GHz. As the functionality of a wave plate is thickness-dependent, we also fabricated the 14- and 21-period sample slabs with the same geometric parameters in Fig. 1(b). Following the analysis stated above, these two samples shall bring  $2\pi$  and  $3\pi$  phase difference between the LEP and REP states, respectively. As such, the sample with 14 periods shall not change the polarization of incident waves, and the functions of the 21-period sample shall be similar to the 7-period one. Calculated and measured transmission spectra shown in Fig. 4(c)  $\sim$  (f) agree with our predictions very well. The functionality of the 7-layered sample rotating the polarization direction of a linear polarized wave is also illustrated in Fig. 4(g) and (h). We can see that the polarization angle of linear polarized wave is perfectly transformed from  $\theta = \pm\pi/4$  to  $\theta = \mp\pi/4$  as predicted.

In conclusion, we have shown that, for metallic helix system, the dispersion branches in different handedness can be tuned independently via separate channels. To the best of our knowledge, this property has not been found in other systems using natural or other artificial materials, and should be attributed to the additional degrees of freedom provided by continuous helical symmetry of metallic helices. By mixing the LEP and REP eigenstates, a metallic helix array can be utilized for the realization of a highly transparent wave plate with an ultra-wide bandwidth. The broadband functionality is conceptually demonstrated in microwave regime. The helix wave plate can be versatile in utility. For example, it can realize the perfect linear-circular polarization transition and the polarization rotation of a



linear polarized light with an angle of  $90^\circ$  at the same broad frequency range. We also note that it is feasible to generalize our findings to other frequency regimes such as THz and even the infrared as well.

This work was supported by NSFC (No. 10974144, 60674778), CNKBRSF (Grant No. 2011CB922001), Hong Kong RGC grant 600209, the National 863 Program of China (No.2006AA03Z407), NCET (07-0621), STCSM and SHEDF (No. 06SG24).

- 
- [1] M. Born, and E. Wolf, *Principles of Optics: Electromagnetic Theory of Propagation, Interference and Diffraction of Light (7th Edition)* (Cambridge University Press, 1999).
  - [2] I. V. Lindell *et al.*, *Electromagnetic Waves in Chiral and BI-Isotropic Media* (Artech House, Norwood, MA, 1994).
  - [3] R. A. Shelby, D. R. Smith, and S. Schultz, *Science* **292**, 77 (2001).
  - [4] J. B. Pendry, *Phys. Rev. Lett.* **85**, 3966 (2000).
  - [5] D. R. Smith, J. B. Pendry, and M. C. K. Wiltshire, *Science* **305**, 788 (2004).
  - [6] J. B. Pendry, D. Schurig, and D. R. Smith, *Science* **312**, 1780 (2006).
  - [7] D. Schurig *et al.*, *Science* **314**, 977 (2006).
  - [8] A. V. Rogacheva *et al.*, *Phys. Rev. Lett.* **97**, 177401 (2006).
  - [9] E. Plum *et al.*, *Appl. Phys. Lett.* **90**, 223113 (2007).
  - [10] T. Q. Li *et al.*, *Appl. Phys. Lett.* **92**, 131111 (2008).
  - [11] N. Liu *et al.*, *Nat. Mater.* **7**, 31 (2008).
  - [12] M. G. Silveirinha, *IEEE Trans Ant. & Prop.* **56**, 390 (2008).
  - [13] J. Pendry, *Nat. Mater.* **5**, 599 (2006).
  - [14] N. Liu *et al.*, *Nat. Photon.* **3**, 157 (2009).
  - [15] J. B. Pendry, *Science* **306**, 1353 (2004).
  - [16] J. K. Gansel *et al.*, *Science* **325**, 1513 (2009).
  - [17] J. K. Gansel *et al.*, *Opt. Exp.* **18**, 1059 (2010).
  - [18] C. Wu *et al.*, *Phys. Rev. Lett.* **105**, 247401 (2010).
  - [19] The  $B_L$  and  $B_R$  branches can be tuned separately by varying the pitch  $p$  only, or alternatively varying both the helix radius  $a$  and  $p$  while keep the ratio of  $a/p$  to be fixed.